An initial comparison of the thermal anomaly detection products of MODIS and VIIRS in their observation of Indonesian volcanic activity

Blackett, M.

Original citation & hyperlink:
Blackett, M. (2015) An initial comparison of the thermal anomaly detection products of MODIS and VIIRS in their observation of Indonesian volcanic activity. Remote Sensing of Environment, volume 171 : 75-82
http://dx.doi.org/10.1016/j.rse.2015.10.002

DOI 10.1016/j.rse.2015.10.002
ISSN 0034-4257
ESSN 1879-0704

Publisher: Elsevier

An initial comparison of the thermal anomaly detection products of MODIS and VIIRS in their observation of Indonesian volcanic activity

Matthew Blackett, m.blackett@coventry.ac.uk

Centre for Disaster Management and Hazards Research, Coventry University, Coventry, CV1 5FB.

Abstract

The Suomi National Polar-orbiting Partnership satellite was launched in 2011. On-board this satellite is the Visible Infrared Imaging Radiometer Suite (VIIRS) with thermal infrared detection capabilities similar those of the earlier Moderate-Resolution Imaging Spectroradiometer (MODIS) sensors of the National Aeronautics and Space Administration Earth Observation System. Fire detection products have been developed using the thermal infrared data for both VIIRS and MODIS and, although having the observation of fire as their main objective, such products are also sensitive to the radiant emissions of active volcanic surfaces, but a comparison of their capabilities in this regard remains outstanding. Here, this comparison is conducted, with a focus on the volcanoes of Indonesia, and findings are initially promising, suggesting that the VIIRS fire detection capability is an improvement over that of its predecessor. For example, between 3 April 2012 and 14 July 2014, volcanic activity was detected on 519 days by the VIIRS product, as compared with 308 days for the MODIS-Aqua product (MYD14). Causes of this apparent enhanced sensitivity are explored and, with the examination of additional data from the MODIS-Terra product and the MODVOLC system, are shown to be the combined influence of spatial resolution, data processing steps, imaging scan width and the fire product algorithm used. As greater quantities of data become available, a more comprehensive comparison of these observations will be possible and will be undertaken at a global scale.

Introduction

In October 2011 the Suomi National Polar-orbiting Partnership (S-NPP) satellite was launched. It was to be an introductory, data collecting satellite for the National Aeronautics and Space Administration (NASA) and the National Oceanic and Atmospheric Administration (NOAA), as part of their Joint Polar Satellite System (JPSS) Mission. With five sensing instruments, including the Visible Infrared Imaging

Radiometer Suite (VIIRS), S-NPP was to provide a continuation in the environmental satellite data record. This record commenced in the late 1970s with NOAA's Advanced Very High Resolution Radiometer (AVHRR) satellites and was most recently added to in 1999 and 2001 by NASA's Moderate-Resolution Imaging Spectroradiometer (MODIS) on-board the Terra and Aqua spacecraft (Schroeder et al. 2014). These sensors each possess infrared detection capabilities which have been harnessed to identify terrestrial thermal anomalies. Although commonly used in observing the characteristic thermal signatures of active fires, such data also have utility in the observation of active volcanic surfaces, and this has been utilised in various applications (e.g. Harris et al. 1998, Wright and Flynn, 2003; Webley et al. 2008, Blackett, 2014). For MODIS, a fire detection algorithm has been developed which utilises its infrared data to produce the Thermal Anomaly/Fire products: MOD14 (for MODIS Terra) and MYD14 (for MODIS Aqua) (Justice et al. 2002, 2006; Giglio et al. 2003). An Active Fire Product (AFP) has also been developed for infrared VIIRS data and using this, and the MOD14/MYD14 algorithm, it also identifies active fires and, as such, any terrestrial thermal anomalies, including those of volcanic origin (Justice et al. 2013; Csiszar et al. 2014).

Volcanic context

Given the huge utility of fire detection products for hazard management agencies on the ground, both MODIS and VIIRS have been compared in terms of their observation of active fires, and initial comparisons have shown consistency in near coincident data, even at varying view angles (e.g. Justice et al. 2013; Csiszar et al., 2014; Schroeder et al. 2014). However, given the higher nominal spatial resolution of the VIIRS, and its enhanced scanning and sampling techniques, a higher sensitivity to thermal anomalies would be expected and indeed, has been confirmed for fires (Csiszar et al. 2014; Schroeder et al. 2014). What is absent in the literature however, is a comparison of the volcanic observational capabilities of the MODIS and VIIRS thermal anomaly products, and that is what this paper seeks to undertake. The chief differences between observing active volcanic surfaces, as compared with fires, are that: 1) the temperature ranges are likely to be higher (with both fresh and cold, or cooling, lava present), 2) the heat sources are likely to be more pervasive and, 3) there is likely to be a greater temperature contrast between hot surfaces and surrounding non-volcanic, high-altitude surfaces.

The comparison conducted here focuses on observations of the volcanoes of Indonesia. This archipelago consists of 78 historically active volcanoes which formed as a result of subduction along the Sunda Arch (Smithsonian Institution 2013). Since the launch of the S-NPP satellite in October 2011, many Indonesia's volcanoes have been particularly active (see Figure 1). In 2012, Mount Semeru erupted and generated multiple pyroclastic flows that warranted a ban on visitors, and Mount Soputan emitted an ash plume that extended 9000 m into the atmosphere (CVGHM, 2012; Darwen VAAC, 2012). Mount Paluweh commenced a period of prolonged activity in early 2013, killing six and forcing evacuations throughout the year and later, in the same year, the eruption of Mount Sinabung forced flight cancellations and the evacuation of 17,000 people (Jakarta Post, 2013; International Business Times, 2013). In 2014, Mounts Kelud and Sinabung erupted, killing tens of people and forcing the rerouting and cancellation of flights (National Geographic 2014; Jakarta Post, 2014); Mount Sangeang Api also erupted, displacing thousands and forcing flight diversions (The Guardian, 2014). The extreme vulnerability of Indonesia to the volcanic hazard is reflected by the fact that two-thirds of the global population exposed to the volcanic hazard are concentrated in Indonesia (UNISDR, 2015).

Sensors and algorithms

The MODIS instruments possess mid- and thermal-infrared bands with a spatial resolution of 1 km at nadir, a swath width of 2330 km and a twice-daily repeat period (Table 1 shows the bands of MODIS). The MODIS Thermal Anomaly/Fire products (MOD14 and MYD14) extract pixels that display the characteristics of thermal anomalies at the surface. These characteristics are based on data from bands 21 or 22 (3.929–3.989 μm), band 31 (10.780–11.280 μm) and the application of a fire detection algorithm initially developed by Justice et al. (2002) and enhanced by Giglio et al. (2003). The algorithm applies background and contextual threshold tests to identify those pixels representing potential thermal anomalies, although the precise algorithm differs marginally between day and night-time applications. The rationale for this difference is that all objects of ambient temperature (including the Earth's surface) emit detectable levels of infrared radiation, even in the absence of solar heating and sunlight. Planck's Law however, determines that emissions from ambient objects

will be greater in the thermal infrared (i.e. band 31) than in the mid-infrared (i.e. bands 21 and 22); the reverse will be true for hotter surfaces. These facts mean that the contrast between hot and ambient surfaces is lower in the daytime, thereby requiring stricter steps to differentiate them from the background. As such, an initial screen is applied in the algorithm whereby thermally anomalous pixels in daytime imagery are identified where the MIR brightness temperature exceeds 360 K, as compared with just 320 K in night-time imagery (Giglio et al. 2003; Justice et al. 2002; Schroeder et al. 2014).

The MODIS fire products are made available in the Hierarchical Data Format (HDF), with its Scientific Data Sets (SDS) listing, amongst other characteristics, the longitude and latitude of anomalous pixels, and the associated fire radiative power (FRP) (Giglio, 2010). The performance of the MODIS algorithm for observing thermal anomalies has regularly been validated by comparison with corresponding Advanced Space-borne Thermal Emission and Reflection Radiometer (ASTER) fire observations both in terms of anomaly detection (Giglio et al. 2003; Morisette et al. 2005; Csiszar et al. 2006) and emission quantification (Giglio et al. 2008).

The VIIRS was developed for cloud and Earth surface observations and initial calibration and validation steps have shown it as performing very well, producing high-quality data comparable with that of MODIS (Cao et al. 2013; Cao et al. 2014). It consists of a panchromatic day-night band and two collections of other bands: five high resolution imagery (I) bands (of 375 m at nadir) and sixteen moderate (M) resolution bands (of 750 m at nadir); the VIIRS bands are compared with each other, and with those of MODIS, in Table 1. Each collection of bands has a 3040 km swath width, providing twice daily global coverage. The I-bands cover the visible spectrum and also include medium and longwave infrared bands. The M-bands cover approximately the same portion of the spectrum (with some shorter wavelength bands) but also possess higher spectral resolution i.e. narrower bandwidths and, with a better signal to noise ratio, are more appropriate for quantitative applications.

Table 1. The bands of MODIS and VIIRS, compared in terms of their spectral characteristics (*dual gain band; † low gain band). The bands outlined are those of relevance to this research.

MODIS			VIIRS					
			Spatial resolution: 750 m		Spatial resolution: 375 m		Spatial resolution: 750 m	
Band	Spectral range (μm)	Spatial resolution (m)	Band	Spectral range (μm)	Band	Spectral range (μm)	Band	Spectral range (μm)
8	0.405 – 0.420	1000	M1	0.402 - 0.422				
9	0.438 - 0.448	1000	M2	0.436 - 0.454				
3	0.459 - 0.479	500						
10	0.483 - 0.493	1000	M3	0.478 - 0.488				
11	0.526 - 0.536	1000					DNB	0.500 - 0.900
12	0.546 - 0.556	1000	M4	0.545 - 0.565				
4	0.545 - 0.565	500						
1	0.620 - 0.670	250			I1	0.600 - 0.680		
13	0.662 - 0.672	1000	M5	0.662 - 0.682				
14	0.673 - 0.683	1000						
15	0.743 - 0.753	1000	M6	0.739 - 0.754				
2	0.841 - 0.876	250	M7	0.846 - 0.885	I2	0.850 - 0.880		
16	0.862 - 0.877	1000						
17	0.890 - 0.920	1000						
19	0.915 - 0.965	1000						
18	0.931 - 0.941	1000						
5	1230 - 1250	500	M8	1.230 - 1.250				
26	1.360 - 1.390	1000	M9	1.371 - 1.386				
6	1628 - 1652	500	M10	1.580 - 1.640	I3	1.580 - 1.640		
7	2105 - 2155	500						
			M11	2.230 - 2.280				
20	3.660 - 3.840	1000	M12	3.610 - 3.790	I4	3.550 - 3.930		
21†	3.929 - 3.989	1000						
22	3.929 - 3.989	1000	M13*	3.970 - 4.130				
23	4.020 - 4.080	1000						
24	4.433 - 4.498	1000						
25	4.482 - 4.549	1000						
27	6.535 - 6.895	1000						
28	7.175 - 7.475	1000						
29	8.400 - 8.700	1000	M14	8.400 - 8.700				
30	9.580 - 9.880	1000						
31	10.780 - 11.280	1000	M15	10.26 - 11.260	I5	10.500 - 12.400		
32	11.770 - 12.270	1000	M16	11.540 - 12.490				
33	13.185 - 13.485	1000						
34	13.485 - 13.785	1000						
35	13.785 - 14.085	1000						
36	14.085 - 14.385	1000						

117

The AFP, which has been developed for the VIIRS, is categorised as an Application Related Product (ARP). An ARP is produced by the S-NPP Ground System's Interface Data Processing Segment (IDPS) which converts the Raw Data Records into geolocated calibrated measurements, or Sensor Data Records (SDRs), and then into Environmental Data Records (EDRs) of geophysical parameters, of which ARPs are a subcategory (Csiszar et al. 2014; Justice et al. 2013). Using the same algorithm as its MODIS forerunner (although Collection 4, as opposed to the Collection 5 currently used in MODIS data), it utilises the suite's mid-infrared and thermal infrared bands (M13: 3.970–4.130 μm and M15: 10.260–11.260 μm), to identify pixels representing thermal anomalies on the surface. Details of the full algorithm, and its similarities and differences to the equivalent MODIS algorithm, are summarised in the product's Operational Algorithm Description (JPSS, 2013). Data from M13 are particularly useful for such studies given its high saturation temperature (634 K) when set in low-gain mode, whereas those of M15 are suitable for characterising the background thermal conditions (although these have the potential to saturate for moderate/large thermal anomalies). Similarly to the MODIS fire algorithm, and with the aim of reducing false alarms, the precise algorithm applied in the daytime is more stringent than the corresponding night-time product. At the current time, only the longitude and latitude of those pixels identified as potential fires are listed within the associated HDF file of the VIIRS AFP, thereby preventing complete comparison with the MODIS data products. However, by the time the first JPSS satellite is launched in 2017, the product will be upgraded to a full Environmental Data Record, with the requirement of a fire mask and FRP data; plans are also in place for updating the algorithm used to the most up to date MODIS Collection 6 version (Csiszar et al. 2014; Schroeder et al. 2014). To date, only one attempt at quantifying thermal emission data retrieved from VIIRS has been made: the Nightfire algorithm (Elvidge et al. 2013). This examines VIIRS Sensor Data Records for anomalies and quantifies the associated thermal emissions, in terms of megawatts, for comparison with MODIS-derived FRP and, using it, a high correlation between MODIS derived FRP data, and VIIRS thermal emissions, has been shown (Elvidge et al. 2013).

Despite the similarity in bands, one important difference in the processing steps between MODIS and VIIRS data is that, prior to being incorporated into a data product, different approaches are taken to

handle the 'bow-tie' effect. This effect is the pixel footprint enlargement and distortion that occurs towards the ends of an image obtained by scanning radiometers such as MODIS and VIIRS. Not only does the 'bow-tie' effect reduce the reliability of pixel comparisons (both within and between scenes) but, by resulting in pixel enlargement towards the end of scan widths, the sensitivity of pixels, for example to fires and thermal anomalies, also degrades towards the scan edge (Wolfe et al. 1998; Cao et al. 2013). To reduce this effect in VIIRS data, a novel approach has been taken which incorporates both the deletion of overlapping pixels, and aggregation of those remaining, based on their distance from the nadir. This approach results in spatial resolutions that are more comparable (to within a factor of two, as opposed nearly five for MODIS), and pixels that approximate a square, across the whole scan (Wolfe et al. 2013; Cao et al. 2014).

Methods

Using the Smithsonian Institution's Global Volcanism Program (GVP) database (available at: http://www.volcano.si.edu/), all Indonesian volcanoes reported to have displayed activity since the availability of the VIIRS AFP (3 April 2012) were identified. These volcanoes, 21 in total, are shown in Figure 1 and all data encompassing elements of this region, for the period 3 April 2012 – 14 July 2014 (835 days and 6754 files), were downloaded from NOAA's Comprehensive Large Array-data Stewardship System (CLASS, www.class.noaa.gov/). For comparison, MYD14 data for the same region and period (6885 files) were downloaded from NASA's Earth Observing System Data and Information System (Reverb, reverb.echo.nasa.gov/). Only MODIS Aqua data were used as its local overpass times (~1.30am and ~1.30pm) are similar to those of S-NPP, thereby facilitating comparison (Csiszar et al. 2014). However, to assist in comparing the performance of the MODIS and VIIRS products, two other datasets were also obtained: 1. MODIS Terra Thermal Anomaly/Fire Product data (MOD14) for the same period and 2. Data from the MODVOLC volcanic detection system (Wright et al., 2004). With regard to MOD14, the differing acquisition times (~10.30am and ~10.30pm), and the rapidly varying nature of volcanic activity and atmospheric conditions, mean its data cannot be directly compared with MYD14 or VIIRS data, but it is included to assist in identifying the causes of any MODIS-VIIRS discrepancies. Data from the MODVOLC system, which uses both Aqua and Terra data, are similarly included to assist in identifying the causes of any such discrepancies.

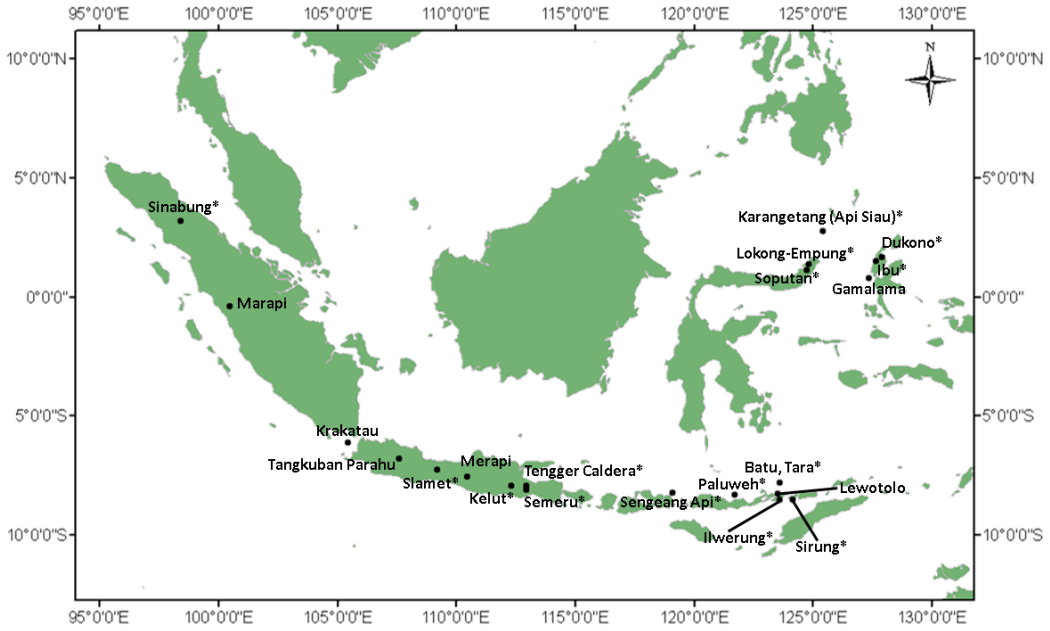

Figure 1. All Indonesian volcanoes recorded as displaying activity according to the GVP database, in the period: April 2012 – 14 July 2014. Asterisks refer to volcanoes which displayed thermal anomalies that were detected in either, or both, the MYD14 and VIIRS fire product files.

The geolocation accuracy of MODIS has been confirmed as around 50 m (Wolfe et al. 2002), and for VIIRS it is comparable, at around 70 m nadir (Wolfe et al. 2013; Cao et al. 2014). Given these small values, extracting data from the respective thermal anomaly product using the longitude and latitude of each volcano will provide the corresponding pixel-level data. However, as thermally anomalous volcanic phenomena may extend far from the crater of a specific volcano (e.g. via lava flow or pyroclastic density current), all thermal anomalies recorded within ±0.02° longitude and latitude of each volcano were identified and extracted to ensure no loss of volcanic signal, while also minimising the possibility of including nearby non-volcanic thermal sources. The signals were organised into daily observations and where there was more than one scene observing the surface on the same day, only data from the scene with the highest summed per-pixel thermal anomaly emission (in the case of MODIS data) or the greatest number of identified anomalous pixels (in the case of the VIIRS AFP and MODVOLC) were considered, so as to avoid compounding the instantaneous daily sum value. To

194 determine the type of volcanic activity potentially responsible for the thermal signals noted, the GVP
195 database was queried for each detected anomaly.
196
197 **Results**
198 *Thermal anomaly detection*
199 An initial comparison of the volcanic-observational capabilities of both the MODIS and VIIRS fire
200 detection algorithms must consist of an examination of their thermal anomaly detection capabilities.
201 Of the 21 volcanoes reported within the GVP database as displaying volcanic activity during the period
202 in question, 15 exhibited thermal anomalies that were detected by either, or both, the MYD14 and
203 VIIRS fire product files (see Figure 1). In many cases, detected anomalies related directly to activity
204 reported in the GVP database, whereas in others, no activity was reported (see Figure 2 for this
205 comparison). Where thermal activity was detected but with no corresponding activity reports, it is
206 likely that either the activity had gone unobserved on the ground or that the thermal activity had a
207 source other than volcanism; conversely, where no thermal anomaly detections were made during
208 periods of reported activity, it is likely that cloud, or volcanic emissions, obscured the surface from
209 view. These discrepancies between observations and recorded activity highlight the relative
210 sparseness of reported volcanic observations in the region which is largely a function of the
211 remoteness and inaccessibility of many of Indonesia's volcanoes.
212
213 In the absence of other truly quantitative data from the VIIRS product, comparison between the
214 MYD14 and VIIRS algorithms can only be extended by examining the presence or absence of
215 anomalies, and by counting the numbers of anomalous pixels identified. Throughout the period, the
216 VIIRS AFP detected 923 anomalous pixels, 62% more than MYD14, which detected 569. The VIIRS AFP
217 also detected anomalies on more days than MYD14 (519 versus 308) and of these days, 26% were
218 also identified as displaying anomalies by MYD14 while in reverse, of the daily MYD14 detections, 45%
219 were also identified by the VIIRS AFP. These data (displayed in Figure 2) suggest a superior detection
220 capability i.e. higher sensitivity to thermal anomalies, for the VIIRS AFP. The discrepancy in detections
221 between these products could be attributed to a number of factors discussed in due course, ranging

from activity type and time of day of observation, to the characteristics of the sensors themselves and how their shared algorithm functions.

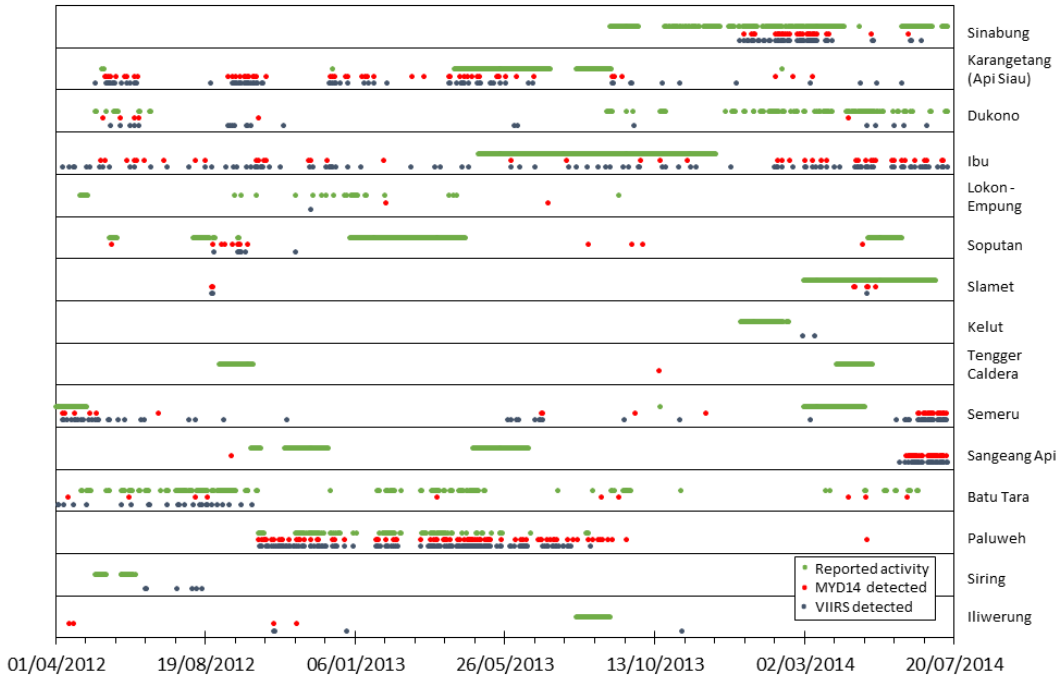

Figure 2. Temporal comparison of GVP reported activity at the volcanoes detailed in Figure 1, with thermal anomalies at them, as detected by MYD14 and the VIIRS AFP, for a period of 835 days (1 April 2012 – 14 July 2014). The interval between minor tick marks on the x-axis is 28 days.

The detection capability of both sensors appears, to some extent, to be dependent on the volcano being observed. At Sengeang for example, of 29 days of VIIRS AFP detections, 86% had corresponding MYD14 detections and, of 30 days of MYD14 detections, 83% had corresponding VIIRS AFP detections; at Paluweh, of 130 days of VIIRS AFP detections, 43% had corresponding MYD14 detections and of 81 days of MYD14 detections, 69% had corresponding VIIRS AFP detections. In other cases however, the VIIRS AFP was shown as much more sensitive for example, at Sirung volcano over the entire period, no MYD14 detections were made, as compared with 6 days of anomaly detection for the VIIRS AFP. Extending this analysis to examine volcanic activity type, Table 2 compares the number of days on which GVP reports of specific types of volcanic activity were made, with the number of days on which thermal anomalies were detected, by product. Confirming a

common theme, the VIIRS AFP more regularly detected thermal anomalies than MYD14, for all activity types. Overall, those types of activity associated with intense heat (i.e. pyroclastic flows, lava flows or explosions) are more comprehensively detected than other activity types, although detections remain low, with only 10.3-16.9% of GVP reports detected by the VIIRS AFP, as compared with 0.0-11.9% for MYD14.

Table 2. The number of days that the VIIRS and MYD14 fire products detected thermal anomalies at Indonesia's volcanoes, as compared with volcanic activity type derived from the GVP database.

	Plume	Seismicity	Incandescence	Lava dome	PF	Fumarole	Lava	Explosion	Ashfall
Days of recorded activity	1276	418	350	297	118	35	29	19	13
VIIRS AFP detected days	135	22	36	37	20	1	3	2	0
Proportion detected (%)	**10.6**	**5.3**	**10.3**	**12.5**	**16.9**	**2.9**	**10.3**	**10.5**	**0.0**
MYD14 detected days	69	19	17	14	14	1	1	0	0
Proportion detected (%)	**5.4**	**4.5**	**4.9**	**4.7**	**11.9**	**2.9**	**3.4**	**0.0**	**0.0**

The difference in VIIRS and MODIS thermal detections between day and night (between which the algorithm used changes) can also be examined. It was found that 64% (n = 364) of all pixels identified by MYD14 as anomalous and 65% (n=601) of all pixels identified as anomalous by the VIIRS AFP, were detected in imagery obtained at night. The significance of this is that there is a comparable, reduced sensitivity of both algorithms during the day-time. This is a function of the higher (and identical) MIR temperature threshold applied within the daytime algorithm.

Thermal anomaly quantification

The detection of volcanic activity, as is possible with both the MODIS and VIIRS fire detection algorithms, is important. Of often greater utility however, is the quantification of such activity so as to provide an indication of the activity type and intensity. For both MODIS and VIIRS products, such quantification is possible by virtue of the number of anomalous pixels identified, as this effectively quantifies the spatial extent of an anomaly; in the case of MYD14 however, quantification is more usefully also is additionally provided by the associated total FRP data. For MYD14, the relationship here between the number of anomalous pixels and total FRP per scene however, is not particularly

strong (r^2 = 0.57). This is because there is a range of FRP values that a pixel identified as anomalous might display. For example, the smallest pixel FRP identified within the dataset was 7.5 MW (for Ibu, 14 June 2012, with no GVP-reported activity) and the largest was 992.3 MW (for Soputan, 18 September 2012, with eruptive activity, including volcanic plumes, reported). The daily sum FRP for all volcanic activity detected is plotted in Figure 3, along with the corresponding daily numbers of anomalous pixels as identified by both MYD14 and the VIIRS AFP. Although in many cases peaks and troughs do coincide, there is only a small positive relationship between both the numbers of pixels identified as anomalous by both sensors (r^2 = 0.28) and between the number of pixels identified as anomalous by the VIIRS AFP and the corresponding MYD14 FRP retrievals (r^2 = 0.15). It is unfortunate therefore, that until upgraded to an EDR, accurately quantifying the emissions detected from the more sensitive VIIRS sensor will remain troublesome.

To assist in determining the cause of the discrepancy in detections between the VIIRS and MODIS fire products, corresponding daily numbers of anomalous pixels, as identified by the MODIS Terra product (MOD14), are also displayed in Figure 3. Although there are similar trends, given the difference in image acquisition time, little relationship exists between either of the variables derived from the Aqua and Terra products (anomalous pixels: r^2 = 0.06, FRP retrievals: r^2 = 0.03) or between the Terra-derived anomalous pixel numbers and those from VIIRS (r^2 = 0.26). MODVOLC detections for the same volcanoes and time period are fewer than those from the MODIS fire products (these data are also in Figure 3). Summed, the number of days that both the MYD14 (308) and MOD14 (386) products made detections is 694 as compared with 520 for MODVOLC (which utilises both MODIS sensors). This difference reflects an acknowledged reduced sensitivity of the MODVOLC algorithm (e.g. Vaughan and Hook, 2006; Blackett, 2013). However for one volcano, Batu Tara, the reverse was found to be true, with MODVOLC making thermal anomaly detections on 145 days, as compared with just 10 for MYD14, 16 for MOD14 and 24 for VIIRS.

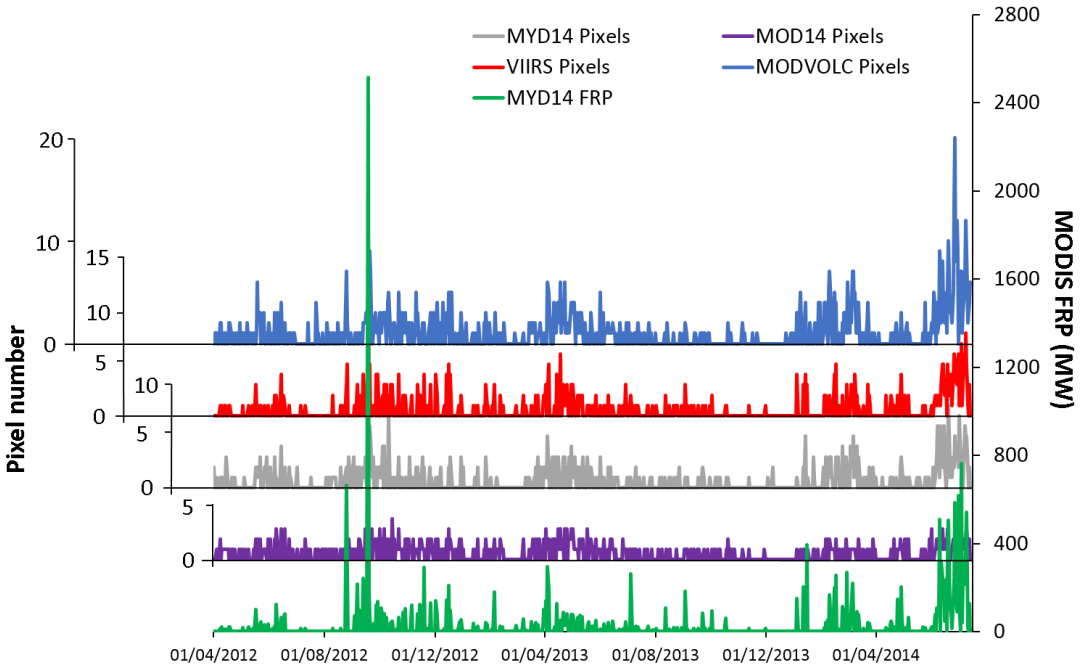

Figure 3. MODIS-derived FRP, and corresponding numbers of pixels identified as anomalous by the MODIS (both MYD14 and MOD14) and VIIRS fire detection products, and also the MODVOLC system.

Discussion

A number of comparable MYD14 and VIIRS fire product detections of volcanic activity have been highlighted however, equally, a number of occasions have been shown with little similarity. Overall, the data suggest an enhanced sensitivity of the VIIRS AFP to smaller and/or more subtle thermal anomalies, as compared with the MYD14 Product. Given that the algorithm used for both products is the same, differences in thermal anomaly detection capabilities must be, primarily, due to variations in pixel size – both physically (i.e. 1000 m compared with 750 m) and by virtue of the data processing (i.e. VIIRS pixel aggregation and sampling scheme). This suggestion is confirmed by the fact that both MODIS Fire Products (MYD14 and [MOD14]), which use the same algorithm and share the same spatial resolution, show a significant anomalous pixel under-detection (i.e. 569 [570]) as compared with the VIIRS AFP (923). Csiszar et al. (2014) showed how the observed differences between the MODIS and VIIRS fire products, in relation to counts of fire pixels, are consistent with those expected due to the differences in spatial sampling *i.e.* given that any terrestrial thermal anomaly will constitute a greater proportion of the footprint of a smaller pixel, the smaller VIIRS pixels would be

expected to detect more, and smaller, thermal anomalies than MODIS, when using a comparable detection algorithm. In relation to the pixel aggregation and sampling scheme that is used in the VIIRS data, it also results in smaller pixel footprints towards the scan edge, further improving spatial resolution here as compared with MODIS (Cao et al. 2013; Justice et al. 2013; Schroeder et al. 2014).

To represent the influence of spatial resolution, Figure 4 shows a range of possible volcanic surface configuration simulations and, based on the infrared emissions that each would produce, the corresponding limits of unsaturated detection (both maxima and minima) for the MODIS and VIIRS sensors (detection will be possible above the maxima but saturation will mean the associated data cannot be reliably quantified). The range of volcanic scenarios that the VIIRS can detect is greater in all respects (up to its pixel size) than for MODIS. The implications of this are that: for a given temperature, the thermal anomaly must be larger to be detected by MODIS; VIIRS can detect cooler anomalies of the same size; and, for anomalies smaller than the pixel size, VIIRS will be able to quantify them up to a greater temperature before saturation (634 K as compared with 500 K for MODIS). Csiszar et al. (2014) confirms that work is on-going to customise the algorithm used in the VIIRS AFP for the specific characteristics of this sensor. An enhanced VIIRS fire detection algorithm has, in fact, already been developed which uses the sensor's 375 m I-bands (bands I4 and I5). This new product shows improved detection performance over the 750 m product (with, for example, a 25× factor increase in absolute numbers of night-time fire pixels detected) (Schroeder et al. 2014). The challenge posed by these smaller pixels however, is that saturation will be more regular (occurring at only 367 K), meaning that it will be quantitatively useful only for smaller and/or cooler thermal anomalies (Schroeder et al. 2014).

The requirement of a VIIRS-specific thermal detection algorithm is confirmed when the MODIS Fire Product data are compared with MODVOLC data. For all volcanoes except Batu Tara, the MODVOLC algorithm predictably underestimated the number of anomalous pixels. For Batu Tara however, the MODVOLC algorithm identified thermal anomalies on 135, 129 and 121 more days than MYD14, MOD14 and VIIRS, respectively. Throughout this period, Batu Tara was persistently active, regularly erupting ash plumes into the atmosphere and displaying Strombolian and effusive activity (BGVN,

2014). The reason for this large difference relates to the water-masking procedure used, and how it is applied in the thermal detection algorithm of the MODIS and VIIRS products. The algorithm requires, in most cases, at least six-valid pixels neighbouring a candidate thermal anomaly; pixels masked as water are invalid (Justice et al. 2006). Given that Batu Tara forms an island (Pulau Komba) of only 4.7 km^2, even when particularly radiant, the MODIS Fire Product algorithm rarely detects a thermal anomaly there as only rarely are there adequate valid pixels; those detected by VIIRS number slightly more as the smaller pixel size means a smaller area of land is required to fulfil the valid pixel requirement. The MODVOLC algorithm in contrast, does not apply this requirement, hence retrieving a larger number of detections. There is clearly therefore, room for improvement in the application of the MODIS and VIIRS fire detection algorithms.

Added to the spatial resolution explanation, one other factor needs to be considered to more fully understand the differing sensitivities of the MODIS and VIIRS fire products: the view scan angle. For the VIIRS sensor, this provides for a swath width of 3040 km, as compared with 2330 km for MODIS. The significance of this difference is two-fold. Firstly, being 30% larger than the MODIS swath, it would be expected that 30% more detections would be made by the VIIRS sensor, thereby explaining a good deal of the 62% increase in VIIRS AFP detections, as compared with MYD14. Secondly, the larger swath means there are no gaps between orbits (i.e. complete global coverage twice daily), as compared with MODIS which experiences gaps in coverage around the equator (Cao et al. 2014). Given that the Indonesian islands are within 10° of the equator, such gaps will have reduced the capability of the MODIS products to view and detect all Indonesian volcanic activity and, as such, will also be partly responsible for the smaller numbers of anomalous pixels detected.

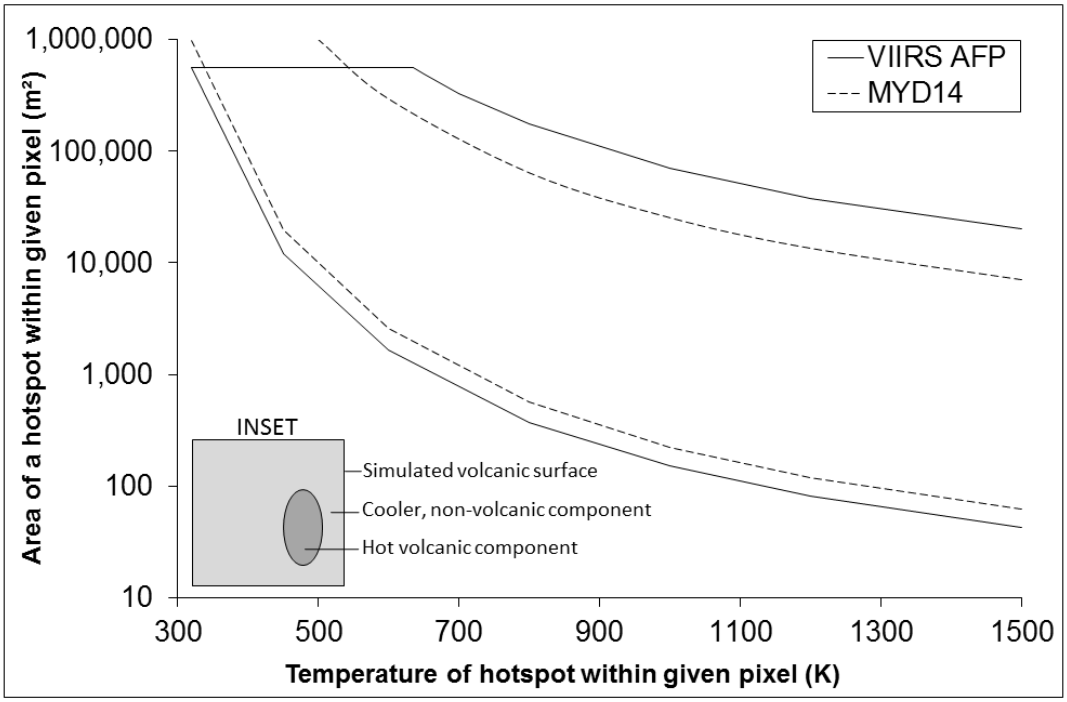

Figure 4. Here, a range of two-component volcanic surfaces are modelled: a hot volcanic component and a cooler, non-volcanic component (this simulated surface is depicted in the inset). The hot component is simulated with a range of temperatures (up to 1500 K, x-axis) and sizes (up to the pixel footprint size, y-axis). Based on the minimum thresholds as prescribed by the fixed threshold fire-detection algorithms, and the maximum unsaturated detection limits of the sensors, points within the envelopes delineated relate to scenarios that, based on the corresponding thermal emissions, the respective sensors and algorithms would be capable of detecting. Above the upper limits represented by these envelopes, thermal activity will still be detected, but saturation will prevent accurate emission quantification. The temperature maxima used here relate to the maximum FRP levels of detection for VIIRS (5100 MW), as compared with MODIS (3500 MW).

Conclusion and the future

It has been shown that comparing the volcanic observational capabilities of two remote sensors is no simple task. The characteristics of the sensors themselves render precise comparison as impossible, and as volcanic activity is sporadic, it is easily missed if the short period of activity is not captured, or if observing conditions are sub-optimal (Csiszar et al. 2014). Equally, the sparseness of reported volcanic observations in Indonesia against which, remote observations might be compared, is

unfortunate and a function of the remoteness and inaccessibility of many of the country's volcanoes. Fortunately, the fact that remote detections have, in some cases, confirmed recorded activity and, indeed in others, have isolated activity not recorded elsewhere, evidences the utility of remotely sensed data, either from VIIRS or MODIS, in filling in the gaps in our knowledge of volcanic behaviour globally and, given its optimal performance, the VIIRS AFP appears most capable in this task.

The data presented have shown that the VIIRS AFP constitutes an improvement over the comparable MODIS product(s) in terms of its sensitivity to, and detection frequency of, volcanic thermal anomalies. This corroborates the findings of a number of other fire-observation studies and should be seen by the thermal remote sensing community as confirming VIIRS as a satisfactory follow-on to the MODIS-era dataset. We are, in fact, lucky to have an extended period of MODIS and VIIRS observations which coincide and against which such comparisons can be made, and from which the influences of the different characteristics of both can be analysed. Users need only wait until 2017 for quantitative VIIRS AFP data to be available against which more thorough comparisons may be made with MODIS. And the future does indeed look promising based on the findings presented here, with VIIRS appearing more sensitive than MODIS and, with a much higher saturation temperature, able to detect and observe a greater range of volcanic scenarios. Researchers additionally have the prospect of an increasingly rich set of new thermally-sensitive satellite sensors to look forward to, with two Sea and Land Surface Temperature Radiometers (on board the European Space Agency's Sentinel-3 satellites) also planned to be operational by 2017. As such, 2017 is likely to be a significant year for the thermal remote sensing community who should, in turn, be optimistic about what it is set to bring in terms of terrestrial thermal anomaly observation.

References

BGVN (2014). Report on Batu Tara (Indonesia). In: Wunderman, R (ed.), Bulletin of the Global Volcanism Network, 39:1. Smithsonian Institution. http://dx.doi.org/10.5479/si.GVP.BGVN201401-264260.

BLACKETT, M. (2013). Review of the utility of infrared remote sensing for detecting and monitoring volcanic activity with the case study of shortwave infrared data for Lascar Volcano from

2001-2005. In: Pyle, D. M., Mather, T. A. & Biggs, J. (eds) Remote Sensing of Volcanoes and Volcanic Processes: Integrating Observation and Modelling. Geological Society, London, Special Publications, 380, http://dx.doi.org/10.1144/SP380.10. The Geological Society of London, 2013.

Blackett, M. (2014). Early Analysis of Landsat-8 Thermal Infrared Sensor Imagery of Volcanic Activity. Remote Sensing, 6, 2282-2295, doi:10.3390/rs6032282.

Cao, C., Xiong, X., Wolfe, R., De Luccia, F., Liu, Q., Blonski, S., Lin, G., Nishihama, M., Pogorzala, D., Oudrari, H. and Hillger, D. (2013), Visible Infrared Imaging Radiometer Suite (VIIRS) Sensor Data Record (SDR) User's Guide. Version 1.2, 10 September 2013, NOAA Technical Report NESDIS 142, Available at https://cs.star.nesdis.noaa.gov/NCC/UsersGuideVIIRS.

Cao, C., De Luccia, F. J., Xiong, X., Wolfe, R. and Weng, F. (2014). Early On-Orbit Performance of the Visible Infrared Imaging Radiometer Suite Onboard the Suomi National Polar-Orbiting Partnership (S-NPP) Satellite. IEEE Transactions on Geoscience and Remote Sensing, 52, 2 1142-1156.

Csiszar, I., J. Morisette and L. Giglio, (2006). Validation of active fire detection from moderate resolution satellite sensors: the MODIS example in Northern Eurasia. IEEE Transactions on Geoscience and Remote Sensing, 44, 7, 1757-1764.

Csiszar, I., Schroeder, W., Giglio, L., Ellicott, E., Vadrevu, K. P., Justice, C. O. and Wind, B. (2014). Active fires from the Suomi NPP Visible Infrared Imaging Radiometer Suite: Product status and first evaluation results. Journal of Geophysical Research – Atmospheres, 119, 803-816.

CVGHM (2012). Center for Volcanology and Geological Hazard Mitigation report in Semeru Weekly Report, Global Volcanism Program. http://www.volcano.si.edu/volcano.cfm?vn=263300.

Darwen VAAC, (2012). Darwen Volcanic Ash Advisory Centre report, in Soputan Weekly Report, Global Volcanism Program. Online: http://volcano.si.edu/volcano.cfm?vn=266030.

Elvidge, C., Zhizhin, M., Hsu, F. and Baugh, K. E. (2013). VIIRS Nightfire: Satellite Pyrometry at Night. Remote Sensing, 5, 4423-4449.

Giglio, L. (2010). MODIS Collection 5 Active Fire Product User's Guide Version 2.4. Science Systems and Applications, Inc. Online: http://www.fao.org/fileadmin/templates/gfims/docs/MODIS_Fire_ Users_Guide_2.4.pdf.

436 Giglio, L., Descloitres, J., Justice, C. O. and Kaufman, Y. J. (2003). An Enhanced Contextual Fire
437 Detection Algorithm for MODIS. Remote Sensing of Environment, 87, 273-282.
438 Giglio, L., Csiszar, I., Restás, A., Morisette, J., Schroeder, W., Morton, D. and Justice, C. (2008). Active
439 fire detection and characterization with the advanced spaceborne thermal emission and
440 reflection radiometer (ASTER). Remote Sensing of Environment, 112, 3055-3063.
441 The Guardian (2014). Volcanic ash cloud from Sangeang Api grounds Australia flights. Online and
442 available at: http://www.theguardian.com/world/2014/may/31/volcanic-ash-cloud-
443 sangeang-api-indonesia-grounds-australia-flights.
444 Harris, A. J. L., Flynn, L. P., Keszthelyi, L., Mouginis-Mark, P. J., Rowland, S. K., and Resing, J. A. (1998).
445 Calculation of lava effusion rates from Landsat TM data. Bulletin of Volcanology, 60, 52–71.
446 International Business Times (2013). Mount Sinabung: 17,000 Evacuated and Hundreds 'Threatened
447 With Starvation' as Volcano Continues to Erupt. Online and available at:
448 http://www.ibtimes.co.uk/mount-sinabung-indonesia-17000-evacuated-refugees-facing-
449 525562.
450 Jakarta Post (2013). Mt. Rokatenda in NTT erupts, reportedly killing five. Online and available at:
451 http://www.thejakartapost.com/news/2013/08/10/mt-rokatenda-ntt-erupts-reportedly-
452 killing-five.html.
453 Jakarta Post (2014). Mt. Sinabung eruptions disrupt flights to N. Sumatra, Aceh. Online and available
454 at: http://www.thejakartapost.com/news/2014/10/11/mt-sinabung-eruptions-disrupt-
455 flights-n-sumatra-aceh.html
456 JPSS (2013). http://npp.gsfc.nasa.gov/sciencedocuments/2013-529/474-00064_OAD-VIIRS-AF-
457 ARP_B.pdf
458 Justice, C.O., Giglio, L., Korontzi, S., Owens, J., Morisette, J.T., Roy, D.P., Descloitres, J., Alleaume, S.,
459 Petitcolin, F., Kaufman, Y. (2002). The MODIS fire products. Remote Sensing of Environment,
460 83:244-262.
461 Justice, C., Giglio, L., Boschetti, L., Roy, D., Csiszar, I., Morisette, J. and Kaufman, Y. (2006). MODIS Fire
462 Products. Algorithm Technical Background Document. EOS ID# 2741.
463 Justice, C. O., Román, M. O., Csiszar, I., Vermote, E. F., Wolfe, R. E., Hook, S. J., Friedl, M., Wang, Z.,
464 Schaaf, C. B., Miura, T., Tschudi, M., Riggs, G., Hall, D. K., Lyapustin, A. I., Devadiga, S.,

Davidson, C., Masuoka, E. J. (2013). Land and cryosphere products from Suomi NPP VIIRS: Overview and status. Journal Geophysical Research-Atmospheres, 118(17), 9753-9765. doi:10.1002/jgrd.50771.

Morisette, J. T., Giglio, L., Csiszar, I. and Justice, C. O. (2005). Validation of the MODIS active fire product over Southern Africa with ASTER data. Int J Rem Sens, 26, 4239-4264.

National Geographic (2014). Indonesia's Mount Kelud erupted this week, sending ash into the air, causing 100,000 people to evacuate and killing three. Online and available at: http://news.nationalgeographic.com/news/2014/02/140214-mount-kelud-volcano-eruption-indonesia-ash-science/.

Schroeder, W., Oliva, P., Giglio, L. and Csiszar, I. B. (2014) The New VIIRS 375 m active fire detection data product: Algorithm description and initial assessment. Remote Sensing of Environment, 143, 85-96.

Smithsonian Institution (2013). The Indonesian Region. Online and available at: http://www.volcano.si.edu/region.cfm?rn=6.

UNISDR (2015). Making Development Sustainable: The Future of Disaster Risk Management. Global Assessment Report on Disaster Risk Reduction. Geneva, Switzerland: United Nations Office for Disaster Risk Reduction.

Webley P. W., Wooster, M. J., Strauch, W., Saballos, J. A., Dill, K., Stephenson, P., Stephenson, J., Escobar Wolf, R. and Matias, O. (2008). Experiences from Real-time Satellite-Based Volcano Monitoring in Central America: Case Studies at Fuego, Guatemala. Int J Rem Sens. 29, 6618 – 6644.

Wolfe, R. E., Roy, D. P and Vermonte, E. (1998). MODIS Land Data Storage, Gridding, and Compositing Methodology: Level 2 Grid. IEEE T Geosci Remote, 36, 1324-1338.

Wolfe, R., Nishihama, M., Fleig, A., Kuyper, J., Roy, D., Storey, J. and Patt, F. (2002). Achieving sub-pixel geolocation accuracy in support of MODIS land science. Remote Sensing of Environment, 83, 31 – 49.

Wolfe, R., Lin, G., Nishihama, M., Tewari, K., Tilton, J. and Isaacman, A. (2013). Suomi NPP VIIRS prelaunch and on-orbit geometric calibration and characterization. Journal of Geophysical Research: Atmospheres, 118, 508-511.

494 Wright R. and Flynn L. P. (2003). Satellite observations of thermal emission before, during, and after
495 the January 2002 eruption of Nyiragongo. Acta Vulcanologica. 15, 67-74.
496 Wright, R., Flynn, LP, Garbeil, H, Harris, AJL, and Pilger, E. (2004). MODVOLC: near-real-time thermal
497 monitoring of global volcanism. Journal of Volcanology and Geothermal Research, 135, 29-
498 49.
499

500 **List of figure captions**

501 Figure 1. All Indonesian volcanoes recorded as displaying activity according to the GVP database, in
502 the period: April 2012 – 14 July 2014. Asterisks refer to volcanoes which displayed thermal anomalies
503 that were detected in either, or both, the MYD14 and VIIRS fire product files.
504

505 Figure 2. Temporal comparison of GVP reported activity at the volcanoes detailed in Figure 1, with
506 thermal anomalies at them, as detected by MYD14 and the VIIRS AFP, for a period of 835 days (1 April
507 2012 – 14 July 2014). The interval between minor tick marks on the x-axis is 28 days.
508

509 Figure 3. MODIS-derived FRP, and corresponding numbers of pixels identified as anomalous by the
510 MODIS (both MYD14 and MOD14) and VIIRS fire detection products, and also the MODVOLC system.
511

512 Figure 4. Here, a range of two-component volcanic surfaces are modelled: a hot volcanic component
513 and a cooler, non-volcanic component (this simulated surface is depicted in the inset). The hot
514 component is simulated with a range of temperatures (up to 1500 K, x-axis) and sizes (up to the pixel
515 footprint size, y-axis). Based on the minimum thresholds as prescribed by the fixed threshold fire-
516 detection algorithms, and the maximum unsaturated detection limits of the sensors, points within the
517 envelopes delineated relate to scenarios that, based on the corresponding thermal emissions, the
518 respective sensors and algorithms would be capable of detecting. Above the upper limits represented
519 by these envelopes, thermal activity will still be detected, but saturation will prevent accurate
520 emission quantification. The temperature maxima used here relate to the maximum FRP levels of
521 detection for VIIRS (5100 MW), as compared with MODIS (3500 MW).
522